Naval Research Reviews

Office of Naval Research
Four/1984
Vol XXXVI

Chemiluminescence

The first underwater, remote controlled, TV camera for exploring at depths of 700 feet (left) and its housing (right). The system, designed with Office of Naval Research funds in 1953 was used for research and salvage until 1973. The picture of the fish was a test photograph taken in 1954. Over the years, research supported by ONR has brought noteworthy advances to underwater photography.

Today these advances permit scientists to study giant marine life on the hot vents of the ocean floor at 9,000 feet below the ocean surface; and the three-man submersible ALVIN, owned by ONR, can descend 13,120 feet to record ocean phenomena with the latest camera equipment.

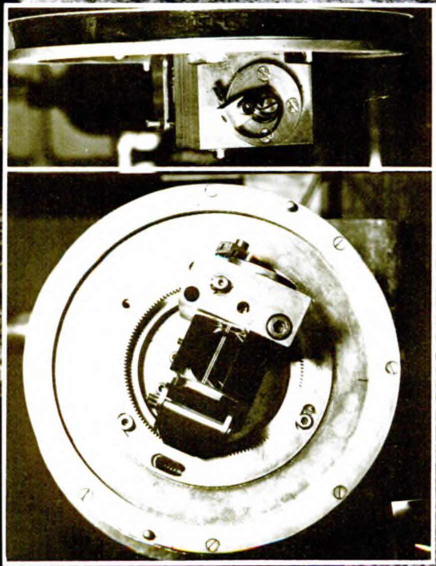

First underwater remote controlled TV viewing system was successfully used to explore the sea bottom for sunken ships and other salvage projects. It was also used to examine the undersides of ships for sea growth and deterioration.

Housing for TV which had to be good up to 700 feet submergence.

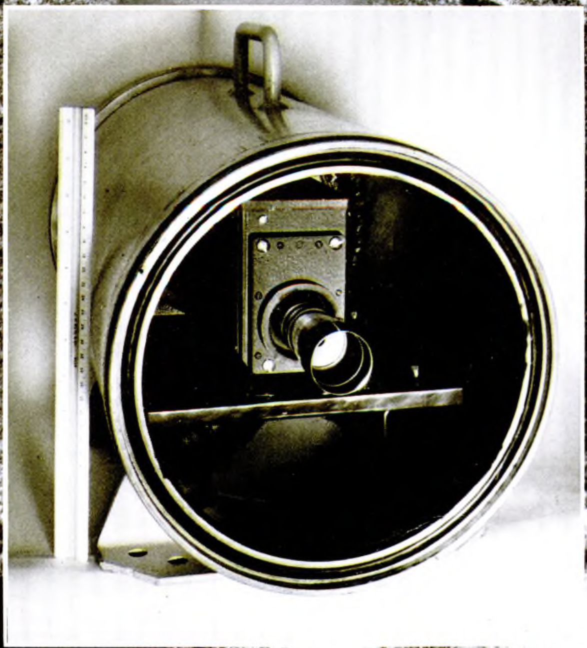

Naval Research Reviews

Office of Naval Research
Four/1984
Vol XXXVI

Articles

Departments

About the Cover

The chemical lightstick illuminating the map is a very popular form of chemiluminescence. Lightsticks are a cold source of energy not dependent on batteries and not ignitable. Many uses include safety and emergency lighting for work at sea as well as field maneuvers. See article on page 16.

Naval Research Reviews publishes articles about research conducted by the laboratories and contractors of the Office of Naval Research and describes important naval experimental activities. Manuscripts submitted for publication, correspondence concerning prospective articles, and changes of address, should be directed to Code 732, Office of Naval Research, Arlington, Va. 22217. Requests for subscriptions should be directed to the Superintendent of Documents, U.S. Government Printing Office, Washington, D.C. 20402. *Naval Research Reviews* is published from appropriated funds by authority of the Office of Naval Research in accordance with Navy Publications and Printing Regulations NAVSO P-35.

GENERAT

View of the ELF receiving antenna as the ship was approaching Grenada. The larger spool consists of 200 turns of wire with a 1.0 meter diameter; the smaller spool is a one turn calibrate loop.

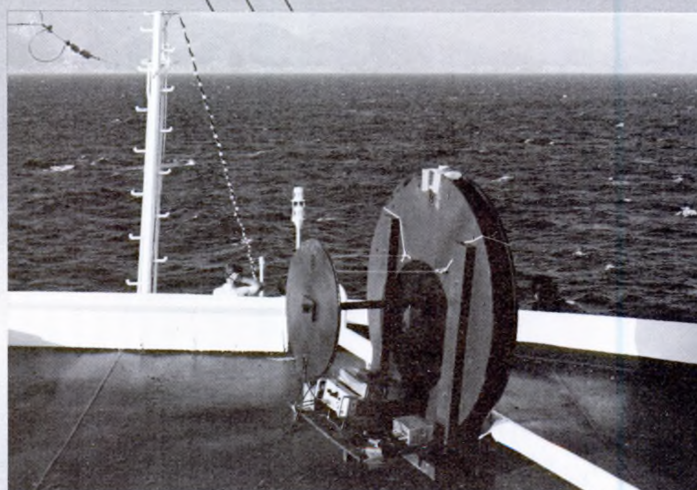

ION of Extremely Low Frequency Radio Waves by High Frequency Electron Heating of the Lower Ionosphere

by
A. J. Ferraro
The Pennsylvania State University

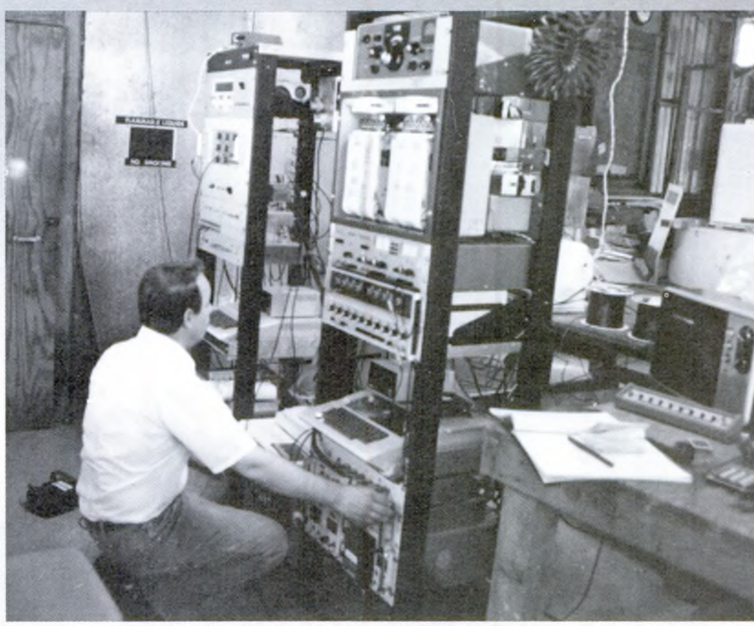

The rack in the foreground is the ELF receiver detector at the receiving site in Los Canos, Puerto Rico. The equipment rack in the background is for diagnositc tests of the ionosphere.

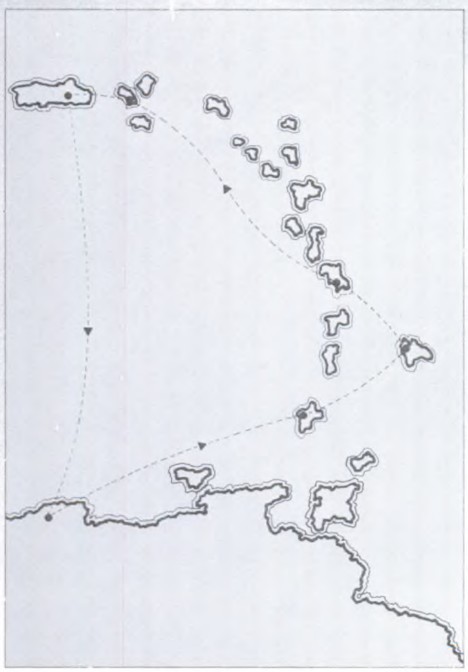

Introduction

Very low frequencies (3-30 Khz, VLF) have played an important role in Naval communications for several years, but extremely low frequencies (less than 3 Khz, ELF) are being introduced today because ELF radio-waves can propagate very long distances with much less attenuation than VLF waves and can penetrate more deeply into sea water.

Difficulties in implementing an ELF transmitting facility are that the wavelengths are very long and to the fact that practical antennas will be electrically small and hence inefficient. For instance, at 100 Hz, a free space wavelength is 3 x 10^6 meters; an antenna wire of 50 Km in length, which is of course physically long, is only a small fraction of the wavelength and would be considered electrically small. Antenna theory shows that electrically small antennas are very inefficient. Even so, an electrically small antenna at ELF poses perhaps a greater problem of locating a convenient site to erect it.

This paper describes ongoing research supported by The Office of Naval Research (ONR) to use natural currents flowing in the lower region of the earth's ionosphere as a transmitting ELF antenna; this would eliminate the site problem but might not necessarily improve the efficiency over a ground-based ELF antenna.

Figure 1

The yearly average of external sq current system.

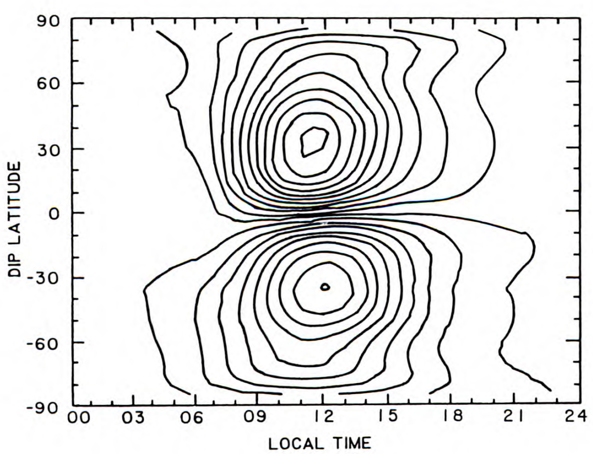

Upper Atmosphere Current System

A brief description of the current systems in the earth's ionosphere will be given. The earth's ionosphere, which consists of free electrons, positive ions, negative ions, and netural particles, is a conducting medium. The upper atmosphere expands and contracts due to solar heating followed by night-time cooling and also due to tidal forces of the sun and moon. Consequently the conducting material moving through the magnetic field of the earth will generate a voltage in the conductor and cause currents to flow similar to moving conductors in an electrical generator or alternator. Because of this, the current system is called the dynamo current system.

Figure 1 shows the yearly average of the current direction for different latitudes and times of day for the dynamo currents.[1] It is clear that the overhead current system can change direction of flow with time of day. For instance, at 60° north latitude, the early morning current direction is north-south, becoming east-west around noon time, and finally south-north in the afternoon. The total strength of current flowing between two adjacent contours is approximately 5,000 amperes. The current flow is counter clockwise in the northern hemisphere and clockwise in the southern hemisphere; therefore, at the equator the current is very intense and is called the equatoral electrojet. At the poles, there is another type of current unrelated to the dynamo system; called the polar electrojet. It results from charged particles from the magnetosphere being dumped into the earth's atmosphere and flowing along the lines of force of the earth's magnetic field. Consequently these currents appear at the polar regions and are responsible for auroral borealis and magnetic storms. Unlike the dynamo currents which are present everyday, the polar electrojet is not predictable but the currents can be more intense at times than the dynamo currents.

The Basic Physics of ELF Generation

The basic physics of the ELF generation is illustrated in Figure 2. This phenomenon involves the irradiation of the ionospheric plasma by a strong high frequency wave which is modulated at some lower frequency Ω. The high-frequency (HF) source consists of very high power transmitters and a high gain HF antenna array resulting in an effective radiated power in the megawatt range. Radio waves with very high power densities can elevate the temperature of the ionospheric electrons several degrees in times of a few microseconds to milliseconds depending upon the altitude being considered. The modulation of the HF signal is shown as a square wave in Figure 2; the temperature (T_e) increases exponentially during the on-time of the HF source and decreases during the off time. The conductivity of the ionospheric plasma is described by a tensor but for

Figure 2

Basic concept of ELF generation.

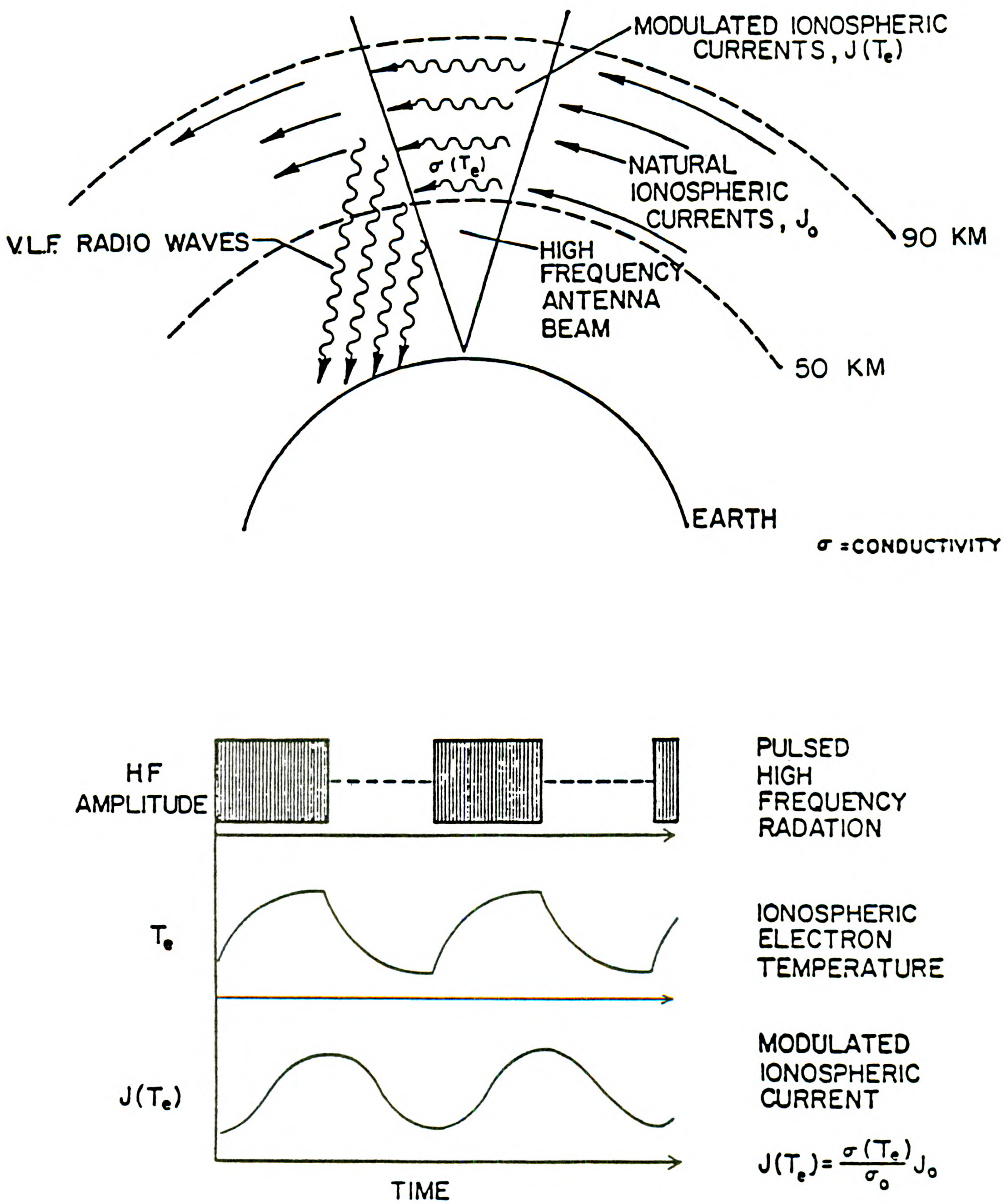

Table 1

Parameters of the Arecibo High Power Facility

Geographic Location	18°N, 67°W
Magnetic Latitude	32°N
Magnetic Dip	51°
HF Frequency	3-12 MHz
Transmiter Power	800 Kw
HF Antenna Gain	23-26 decibels
Antenna Beamwidth	5°-10°
Effective Radiated Power	160-320 megawatts

simplicity of explanation let it be considered a simple resistance which is temperature dependent. The ionospheric region which is heated by the HF antenna beam shown in Figure 2 has its resistance modulated with the same period as the temperature, i.e., corresponding to frequency Ω. Consequently the natural ionospheric currents passing through the heated volume will also be modulated with frequency Ω as illustrated in the bottom waveform of Figure 2. Thus through HF heating, dynamo currents, which are almost D.C., are converted to A.C. currents of frequency Ω. These A.C. currents occupying the heated volume are the sources of electromagnetic waves of frequency Ω which radiate into the region between the earth's surface and the lower ionospheric boundary and propagate long distances via the waveguide formed by the two boundaries.

Unlike a ground-based ELF facility, the ground-based HF facility required with this technique, has wavelengths that are many times smaller so that it is much easier to implement the HF antenna array and portable facilities may even be considered.

Figure 3

Relative power at 70 km for 5.1 MHz.

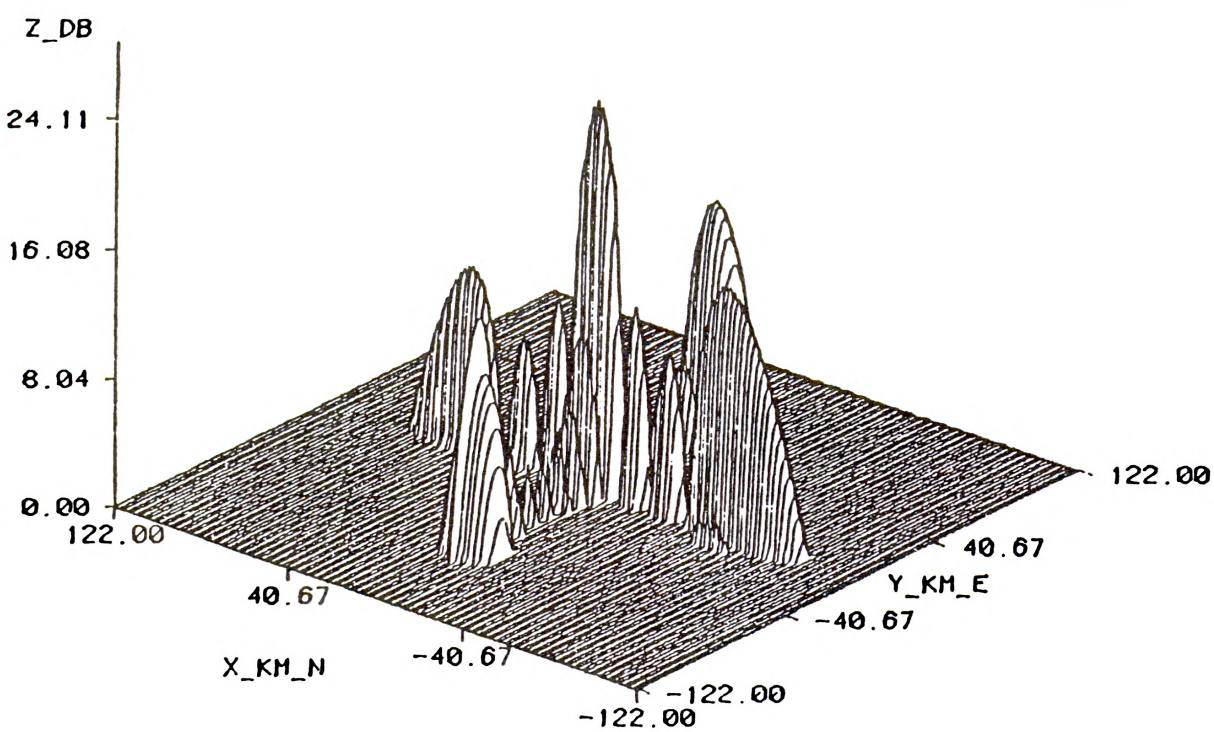

The High Power HF Facility

To prove the capabilities of the ELF antenna using modulated natural currents, the high power HF facilities of the Arecibo Observatory, Arecibo, Puerto Rico were used. Table 1 summarizes the pertinent parameters of this facility.

In evaluating the radiation properties of the ELF ionospheric antenna, it is important to determine carefully the radiation pattern of the HF antenna system, which consists of 32 orthogonal non-planar log-periodic dipole arrays. Figure 3 shows calculated power density in a plane at 70 km altitude for an HF frequency of 5.1 MHz[2]; note the presence of the stronger main beam and side lobes. All lobes contribute to modulating the ionospheric conductivity, so one can view the ELF ionospheric antenna as multiple ELF current sources. Analysis of the resulting ELF signal strength on the ground directly beneath the ELF ionospheric antenna as a function of ELF frequency is presented in Figure 4 for HF frequencies of 3.17 and 5.1 MHz. The sweep-frequency response is significantly different for the two HF frequencies due to the partially destructive interference from the multiple ELF sources created by the side lobes and main beam of the HF antenna. Figure 2 depicted only heating from a main beam but Figures 3 and 4 show realistic performance from a practical HF antenna.

In the design of an HF facility to utilize the ionospheric antenna for a potential communication system, proper attention must be given to the HF array to optimize operation at the desired ELF frequency.

Description of the ELF Receiving Facility

Research proceeded under the following general categories:

(a)Detection of ELF/VLF radiation due to modulation of the dynamo, polar electroject and equatorial electroject current systems.

(b)Characterization of the ELF source.

(c)Medium range propagation (<1000km) from the ionospheric antenna.

(d)Long range propagation from the ionospheric antenna (Tromsø, Norway to University Park, Pennsylvania).

A more complete description of the receiving system and its calibration was described in Ferraro et al.[3] Briefly the receiver system is a tuned ELF receiver employing synchronous detection. The in-phase and quadrature outputs of the synchronous detector, along with the automatic gain control (A.G.C.) voltage from the HF monitor receiver, are sampled by the data acquisition system and recorded on magnetic disk. The A.G.C. voltage from the HF monitor receiver is recorded in order to define the "heater" on-off status; only simply coded transmissions were used initially, generally 2 minutes of on time for the heater followed by 2 minutes of off time. A receiving loop antenna is used that is 1 meter in diameter consisting of 200 turns and having a tuned Q of approximately 55 at 2500 Hz. A small 0.5 meter diameter one-turn calibration loop is located coaxially at a distance of 0.5 meter from the main loop. Outputs from the synchronous detector can be used to calculate both magnitude and phase of the ELF radiation; unlike modulation of the polar electroject, good phase stability can be observed on numerous occasions from the modulation of the dynamo current system. As will subsequently be shown, this phase stability makes determination of the height of the phase center of the ELF antenna source possible.

Observations of ELF Generation from Ionospheric Heating

Observation of ELF generation has been positively associated with ionospheric heating by using cross-modulation as a diagnostic tool.[4]

Figure 4

ELF radiation frequency response.

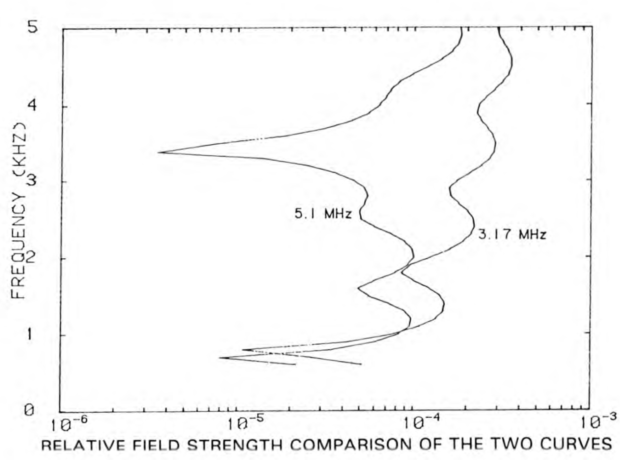

Figure 5

September 7, 1982 loop rotation test.

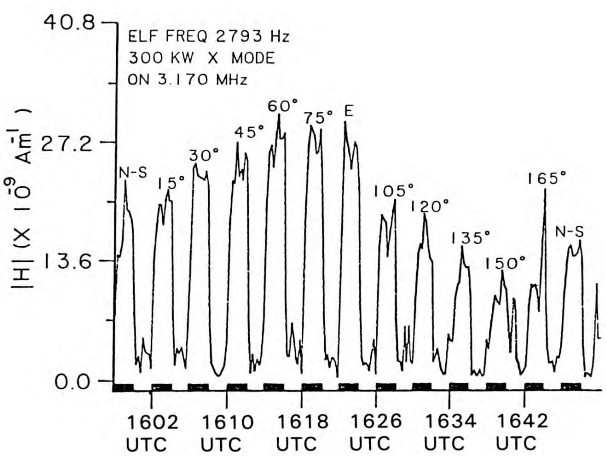

Figure 6

Phase height experiment.

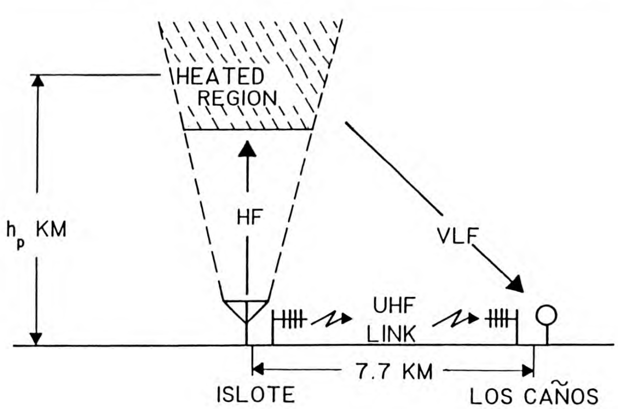

Measurement of the polarization characteristics (axial ratio and tilt angle of the ellipse) at ELF frequencies was determined from loop rotation observations. The direction of the horizontal dynamo currents will change with time of day as discussed earlier and so will the direction of the ELF currents.

Figure 5 shows slow scan-loop rotation data (ELF signal level) for an ELF frequency of 2793 Hz from with axial ratio and tilt angle of the polarization ellipse can be computed. The darkened strips are time intervals when the modulated HF source was turned on for 2 minutes while the blank periods represent off periods for 2 minutes. These data are measured essentially directly beneath the ELF ionospheric antenna and are referred to as local data.

Several observations were devoted to measuring the height of the ELF source. Since the ELF current distribution is a function of altitude depending upon the electron temperature height distribution,[5,6] only a height corresponding to the phase-center of the ELF source is possible. Furthermore the ELF signal is assumed to propagate at the speed of light so this height will correspond to the phase height. In the remainder of this paper, the term "height" will mean phase height (h_p) of the phase-center of the ELF antenna.

Figure 6 shows the simple geometry of the height experiment; here the ELF receiver is located at Los Canos which is 7.7 km from the location of the "heater" at Islote. A UHF link is used to send the modulation waveform at the transmitter site (Islote) to the receiver site (Los Canos) and it is applied to the calibration loop of the ELF receiver loop during the heater off cycles. The ELF ionospheric antenna phase can be observed in most cases. Table 2 shows calculated heights, h_p, for different ELF/VLF frequencies.

Table 2

Phase Height vs ELF/VLF Frequency

Date	Time (LMST)	Freq.	hp (km)
9/2/82	1211-1218	2000 Hz	77.4
9/2/82	1200-1204	2293 Hz	76.5
9/7/82	1232-1243*	2500 Hz	73.9
9/2/82	1120-1130	2793 Hz	62.3
9/2/82	1220-1226	3144 Hz	53.9

Power = 400 kw except * = 200 kw

The interesting feature is that higher modulation frequencies have lower phase centers. It is well established that the time constants for heating and cooling of the lower ionosphere are shorter at lower altitudes,[5] and therefore it is expected that the higher modulation frequencies will return from lower altitudes as shown in Table II.

Figure 7 shows data (ELF signal level) with different power levels from the HF heater facility transmitters while Figure 8 shows the effect of HF heater duty cycle; the duty cycle is the percentage of HF on time to the sum of on and off time. The results confirm the linearity of ELF radiation for the power levels available and establishes a detectable ELF signal with only 20 Kw of transmitter power. The duty cycle test shows that small duty cycles allow insufficient time for maximum heating to occur; hence the change in electron temperature, and consequently ELF radiation intensity, will be smaller. Likewise, larger duty cycles leave insufficient time for the medium to cool so the electron temperature change is smaller. At the HF power densities used in these experiments, the time constant for heating is slightly different than the time constant for cooling; is it shown theoretically that a duty cycle of about 48 percent would maximize the ELF radiation intensity.

An initial attempt was made to measure ELF radiation at a very low ELF of 89 Hz during measurements at Arecibo in March 1983. Because the ionospheric antenna is such a small fraction of a wavelength, the field intensity received is considerably smaller than the data shown in Figure 5. Detection of the signal requires a spectral analysis using the Fast Fourier Transform (FFT) to establish the presence of a 240 second period (2 minutes on −2 minutes off). Figure 9 shows the result of the FFT applied to the data which seems to clearly indicate the presence of the 89 Hz component marked by the arrow. A 240 second period corresponds to a spectral line at 1/240 Hz or .00417 Hz. This measurement was made 7.7 km from the HF heater facility.

Longer Range Propagation of ELF Radiation

Data presented thus far have been locally received. Because the received signal is stronger, it is clearly defined from the coded on-off pattern of the HF facility. At longer propagation ranges, the signal-to-noise ratio can prevent direct observation; in these cases a spectral analysis (FFT) is used. Propagation range has been classified as medium range (<1000 km) and long range (>1000 km).

Medium range detection of ELF radiation was conducted in two ways; one was at a land-based receiving station only 50 km distant and the second was aboard a

Figure 7

April 1, 1982 power level test.

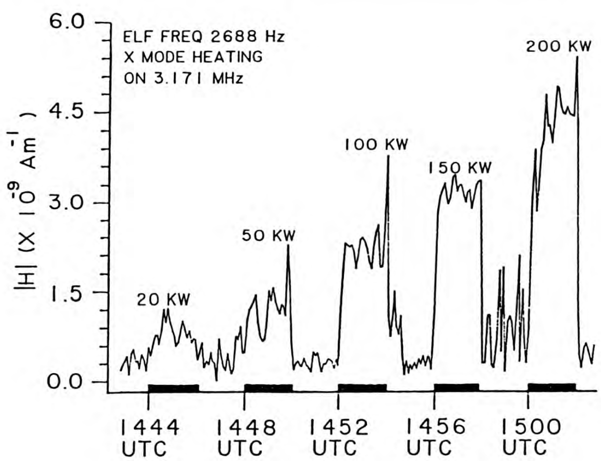

Figure 8

Relative field strength vs HF duty cycle test; September 3, 1982 at 2793 Hz.

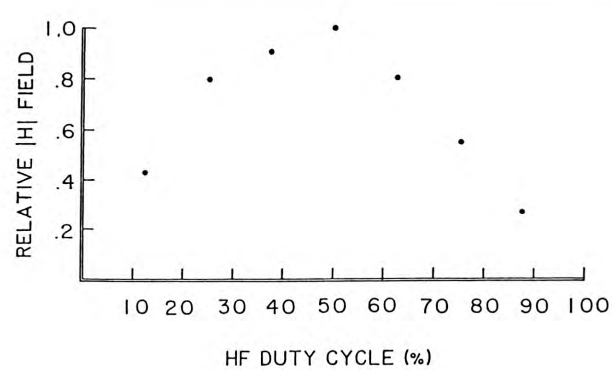

Figure 9

Detection of 89 Hz radiation at Los Canos, Puerto Rico.

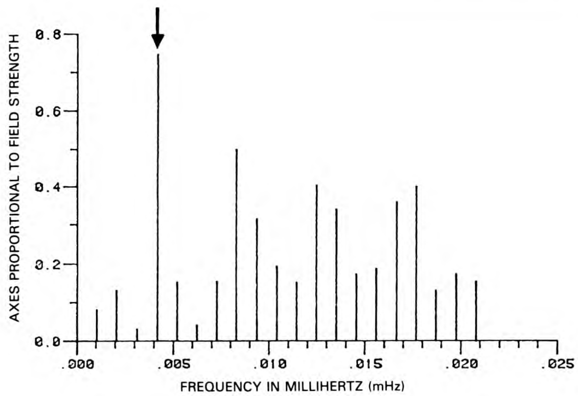

Figure 10

Map of route during shipboard experiment.

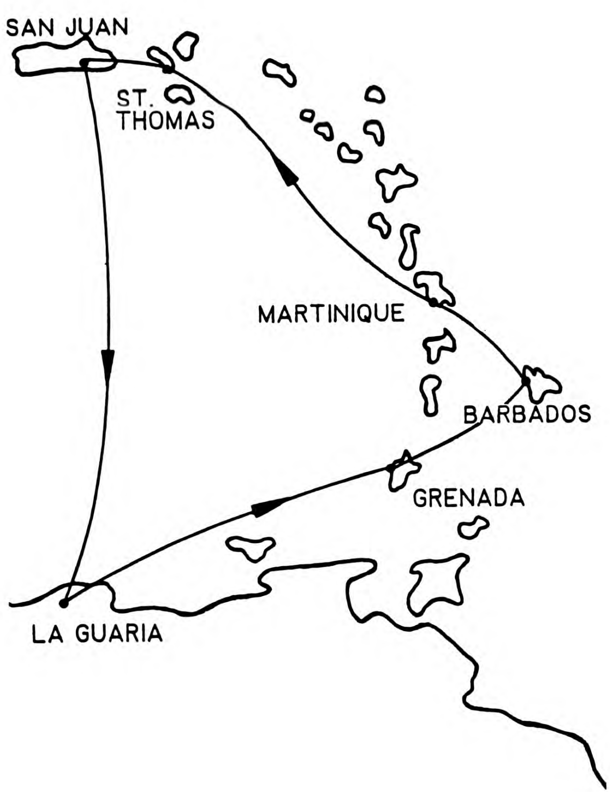

ship with range less than 1000 km. In the first case, the range was small but the sweep frequency characteristics of the ELF source were considerably different from local results; this provided further verification of our model of multiple ELF sources as discussed earlier. In the second case, ship measurements provided an inexpensive method of examining the waveguide model we are studying. During ship measurements, a second receiver at Arecibo was used for local measurements so that waveguide attenuation could be calculated between the two receiver sites and waveguide injection could be estimated from local measurements.

Geographical route of the shipboard experiment is shown in Figure 10. Throughout the experiments, several measurements were made with varying VLF/ELF frequencies, distances and time of day. Figures 11a through 11c show definite presence of VLF/ELF signal spectral components indicated with arrow heads. 4.17 mHz represents a 240-second period resulting from the 2-minute on and 2-minute off HF heater operation. Detailed parameters of the measurements are summarized in Table 3.

Table 3

Shipboard Parameters

Figure	11a	11b	11c
Frequency	2793 Hz	5000 Hz	996 Hz
Receiver Site	Laguaria, Ven.	Martinique	Martinique
Distance	872 km	741 km	741 km
Time (LMST)	0900-1000	1100-1200	1300-1400

The positive results of medium range shipboard measurements discussed above are very encouraging.

Only limited long-range propagation measurements have been made at this time, with the limited purpose of showing the feasibility of detection. Refer to Figures 6a, 6b and 6c,[3] which show reception of 2 KHz signals from Tromsø, Norway coinciding with the presence of polar electroject currents as identified from magnetometer records.

It is the primary objective of this research to evaluate intensely the long-range communications from the ionosphere antenna using the dynamo current system, and this is currently under study with a propagation path from Arecibo to University Park, Pennsylvania.

Figure 11a

Detection of 2793 Hz ELF radiation at Laguaria.

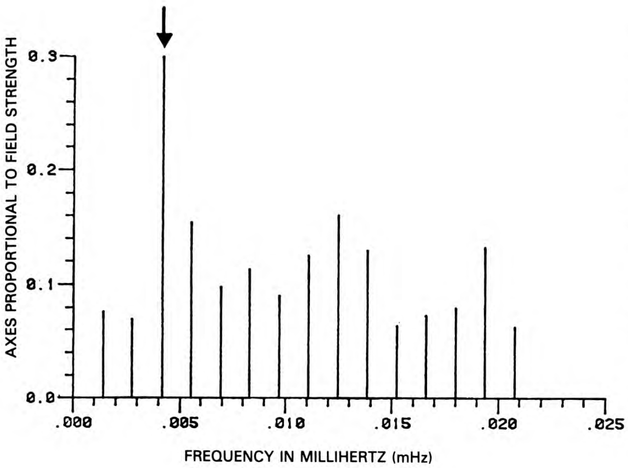

Figure 11b

Detection of 5000 Hz ELF radiation at Martinique.

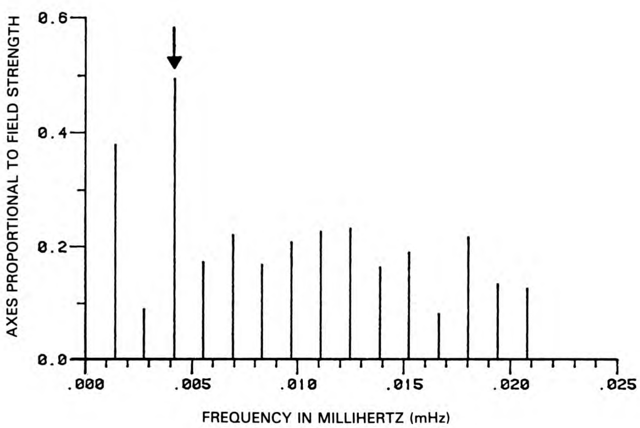

Figure 11c

Detection of 996 Hz ELF radiation at Martinique.

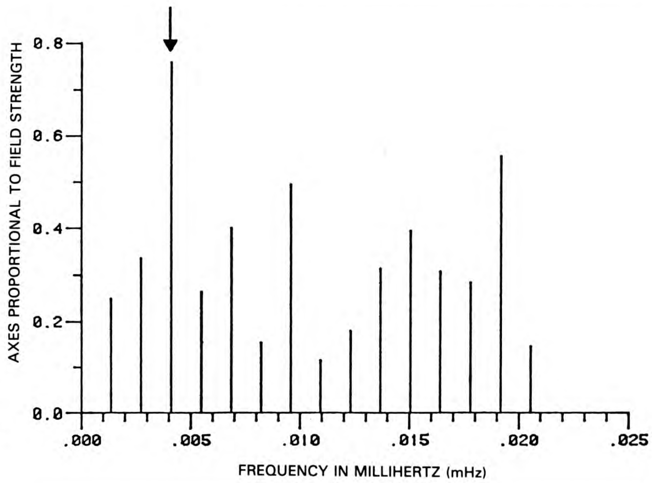

Some Theoretical Concepts

A rather simple but informative analysis is presented in this section as a guide in optimizing the preferred ELF frequency to conduct testing. In this model, a parallel plate waveguide geometry is used, as shown in Figure 12. For $Z>h$ is a semi-infinite region of constant ionization and collision frequency with the ELF source imbedded in it at $Z=h_1$. The region $0<Z<h$ is the free space region of the waveguide. The region $Z<0$ will be either earth or sea water. For ground-based reception, a receiving loop is placed at horizontal range X_o and $Z=0$; but for receiving below the ocean surface, a receiving loop is located at horizontal range X_o and depth $= -Z_1$.

The objective of this study is to determine the total loss in field intensity at depth $-Z$, relative to the field intensity the source delivers to the upper waveguide wall. The propagation loss within the guide is calculated with waveguide theory,[7] and the field intensity injected into the waveguide requires calculation of the ionospheric—air transmission loss. Attenuation in sea water and transmission across the air-sea boundary can be obtained by a straight forward calculation.[8]

Figure 13 is the total system loss for one megameter range at various depths below the ocean surface. It is clear that there is an optimum ELF frequency for each depth; lower frequencies are required for greater depths. For ground-level receivers, 5KHz is optimum (figure not shown for that case). Initial ELF testing between 2-5 KHz will be conducted before the lower frequencies are tried in order to insure a greater possibility of detection.

Discussion

This paper has provided a brief summary of research being conducted to use the dynamo current system for an ELF antenna. It has been clearly established that measureable ELF waves can be observed locally, and on medium and longer range propagation paths. The dynamo current system provides a consistent, reliable source which can be conveniently modulated by a high power HF source. The feasibility of reliable long path detection of information is currently being studied.

Figure 12

Geometry of ELF/VLF communication system using ionospheric ELF/VLF source.

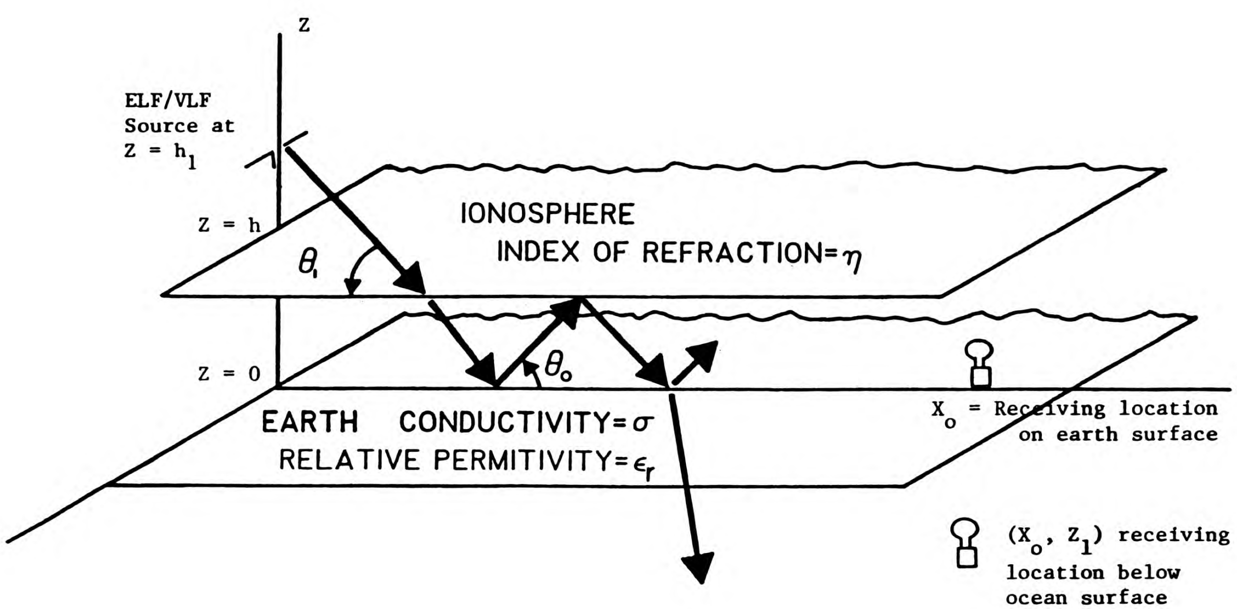

Figure 13

Total system loss.

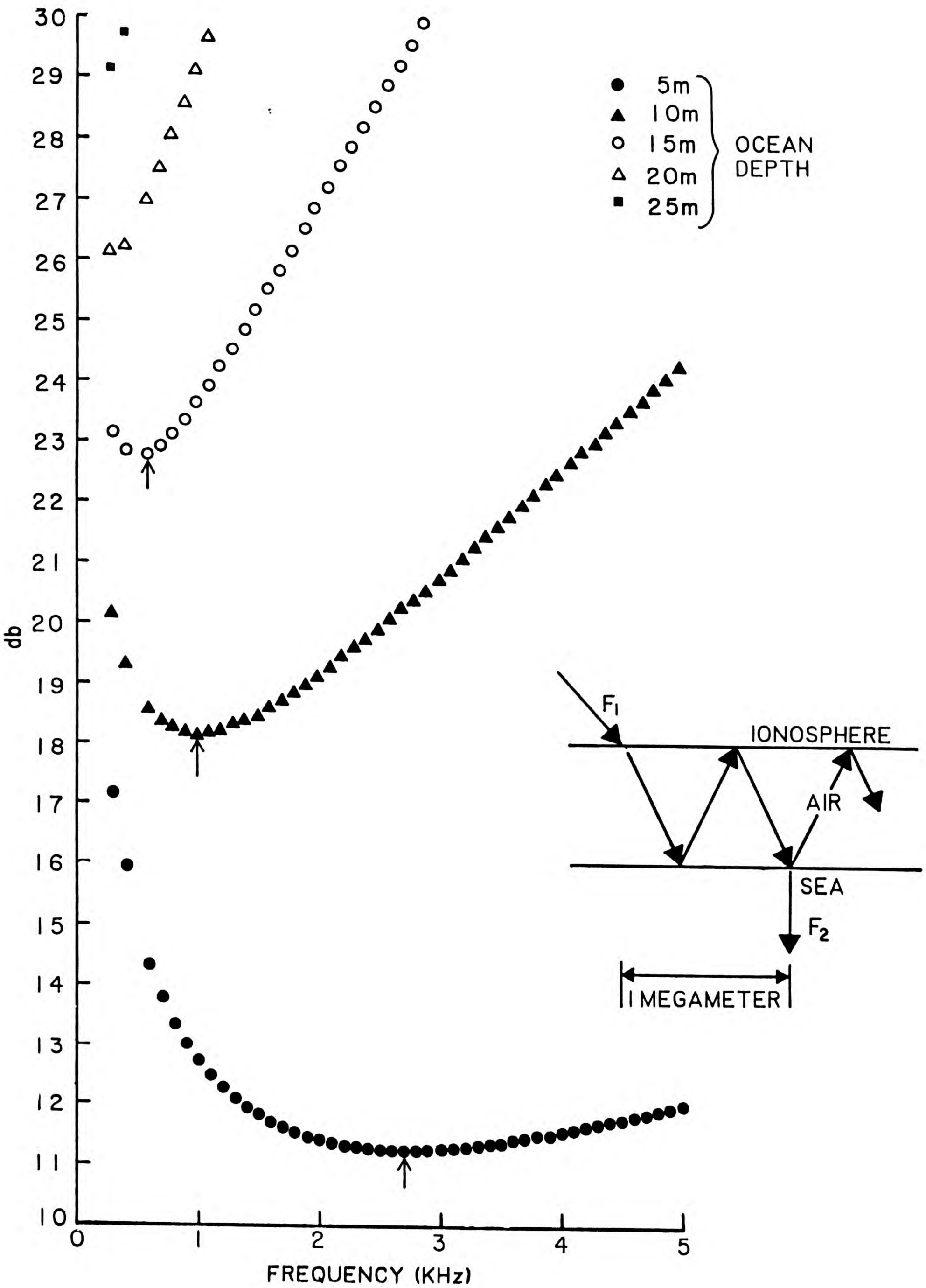

Since this paper was originally written, two new developments have occurred. (1) Information in the form of a binary coated message has been transmitted over the path from Arecibo, Puerto Rico, to University Park, Pennsylvania, and successfully decoded at the receiving station. (2) The rather simple theoretical analysis described in the previous section has been recalculated for a more realistic ionospheric model; and it is now possible to predict ELF field strengths at any receiving location from an ionospheric atenna at any latitude and longitude desired.

References

1. Matsushita, S., *Radio Science,* 4 (1969) p. 771.
2. Carroll, K. J., A. J. Ferraro, H. S. Lee, R. Allshouse, B. Long, and R. J. Lunnen, Report PSU-IRL-SCI-475, Ionosphere Research Laboratory, Pennsylvania State University, University Park, Pennsylvania (1983).
3. Ferraro, A. J., H. S. Lee, R. Allshouse, K. Carroll, A. A. Tomko, F. J. Kelly, and R. G. Joiner, *Journal of Atmospheric and Terrestorial Physics,* 44 (1982) p. 1113.
4. Ferraro, A. J. H. S. Lee, J. N. Rowe, and A. P. Mitra, *Journal of Atmospheric and Terrestorial Physics,* 36 (1974) p. 741.
5. Tomko, A. A., Report PSU-IRL-SCI-470, Ionosphere Research Laboratory, Pennsylvania State University, University Park, Pennsylvania (1981).
6. Richardson, C., Report PSU-IRL-Memo-1, Ionosphere Research Laboratory, Pennsylvania State University, University Park, Pennsylvania (1982).
7. Budden, K. G., *Radio Waves in the Ionosphere,* Cambridge University Press (1966) pp. 42-46.
8. Jordan, E. and K. Balmaira, *Electromagnetic Waves and Radiating Systems,* second edition, Prentice Hall (1968).

Acknowledgements

The results presented in this paper have had the dedicated assistance of Dr. H. S. Lee, Professor of Electrical Engineering, Mr. Roger Allshouse, Mr. Kenneth Carroll, Mr. Raymond Lunnen, Ph.D. candidates in Electrical Engineering at The Pennsylvania State University, and Mr. Thomas Collins, Director of Electronic Services. The Arecibo Observatory is operated by Cornell University under contract to the U.S. National Science Foundation.

Author

Dr. Anthony J. Ferraro is Professor of Electrical Engineering at the Pennsylvania State University. His research and publications have been primarily in the field of ionospheric modification, radio wave propagation, ionospheric physics, and electromagnetic theory. Dr. Ferraro is a contractor of the Office of Naval Research studying generation of extremely low frequency radio waves.

Profiles in Science

Professor Mildred S. Dresselhaus

holds the Abby Rockefeller Mauze Chair in Electrical Engineering and Computer Science and Physics at Massachusetts Institute of Technology and is affiliated with the Center for Materials and Engineering, MIT, which she formerly directed. Currently, she is President of the American Physical Society and serves on numerous advisory committees of the National Research Council and other Federal agencies. She has been active in the study of a wide range of problems in the physics of solids; in the areas of semiconductors, semimetals, and metals she has an international reputation. As a Principal Investigator of the Office of Naval Research, her work has been directed toward the modification of the properties of electronic materials and graphite fibers by intercalation and implantation. Professor Dresselhaus is a member of the National Academy of Sciences and a Fellow of the American Academy of Arts and Sciences as well as the American Physical Society.

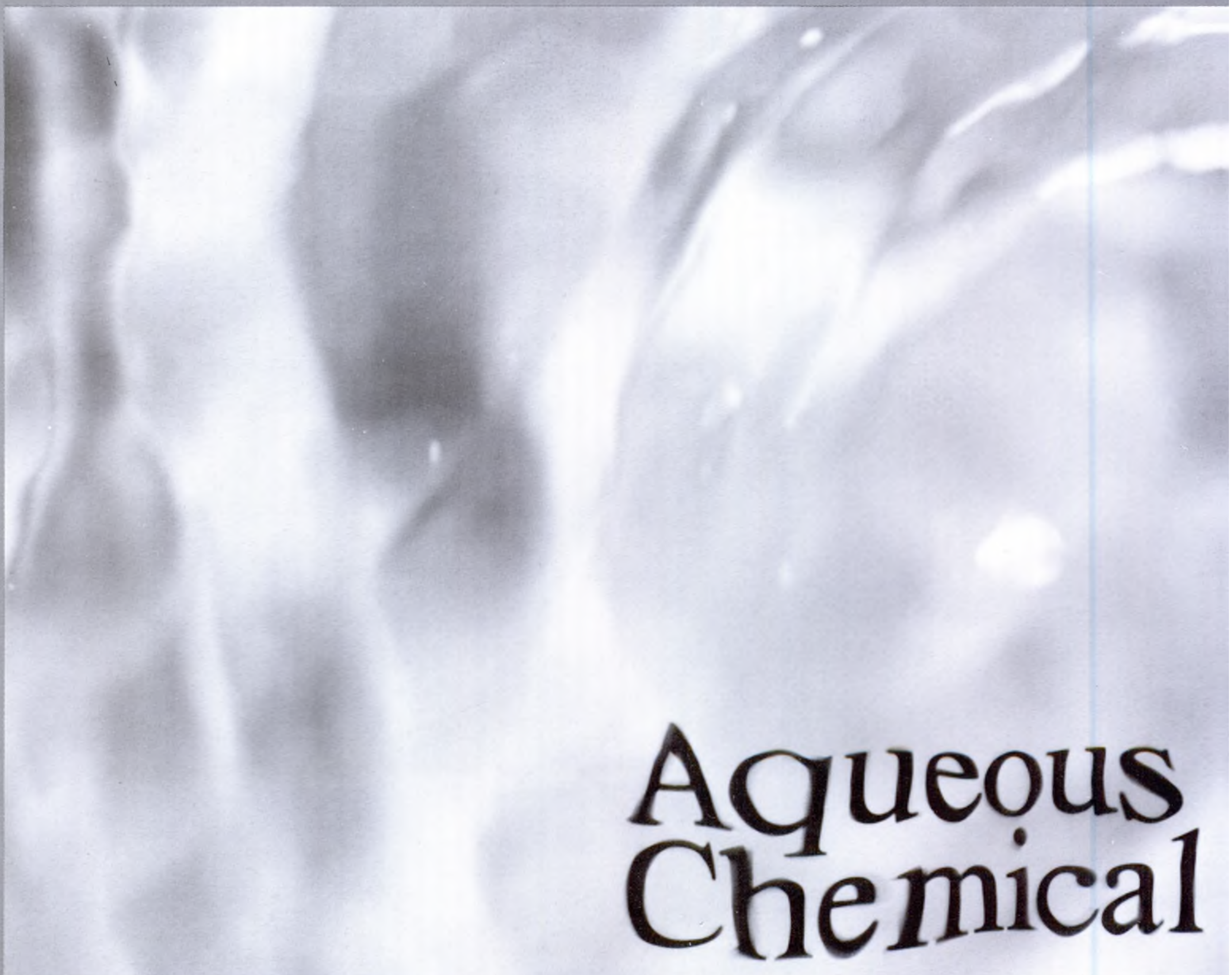

Aqueous Chemical Light
A NEW HORIZON

One of the most fascinating displays of chemical energy in action is the phenomenon of chemiluminescence; the conversion of chemical energy into electronic excitation, apparent as visible light emission. The most efficient of any of the known non-enzymatic chemiluminescent systems involves the reaction of hydrogen peroxide with certain derivatives of oxalic acid in the presence of a fluorescent substance.[1] This class of reactions involves an initial attack of hydrogen peroxide on an oxalic ester or amide generating a peracid intermediate (*1*) which undergoes further reaction to yield a key chemiluminescent intermediate which was originally proposed by Rauhut to be the dimer of carbon dioxide, 1,2-dioxetanedione (*2*).

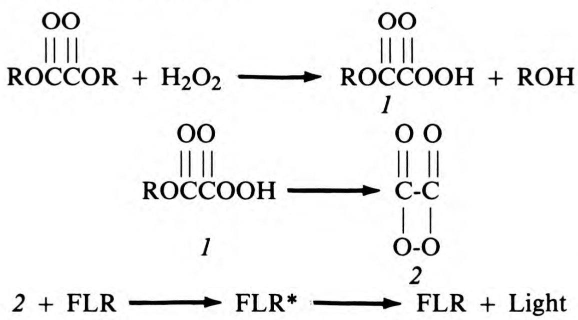

This highly energetic key intermediate then interacts with a separate fluorescer molecule possibly by way of the CIEEL mechanism[2] to generate the excited state of the fluorescer (FLR*), which then emits light in a typical fluorescence decay process.

The peroxyoxalate chemiluminescent reaction differs from most other known liquid-phase chemiluminescent reactions in that a separate energy transfer step from an energetic key intermediate to a fluorescent molecule is involved. This allows the color of the emitted light to be selected by choice of the appropriate fluorescer. An additional advantage of separating the chemical reactants from the emitting molecule is that structural features unique to each part of the system can be incorporated into separate molecules thereby facilitating the optimization of the chemiluminescent system.

BY
Arthur G. Mohan
Seton Hall University, New Jersey
and
Michael M. Rauhut
American Cyanamid Co.
Stamford, Connecticut

The first example of a chemiluminescent reaction involving an oxalic acid derivative was reported by Chandross[3] who found that treatement of oxalyl chloride with hydrogen peroxide in the presence of a fluorescent molecule, 9,10-diphenylanthracene, gave a very bright but short-lived emission corresponding to the fluorescence of the hydrocarbon. Subsequent research at American Cyanamid with support from a number of governmental agencies including the Office of Naval Research led to a highly efficient chemiluminescent system with record high quantum yields.[4]

The practical aspects of the peroxyoxalate chemiluminescent system has become of increasing importance in recent years in both the military and civilian sectors. A number of chemiluminescent devices are now being marketed by the American Cyanamid Company under the CYALUME trademark throughout the entire world. The CYALUME lightstick is a plastic tube containing the oxalic ester and the fluorescer in an organic solvent in which floats a smaller glass tube containing a dilute solution of hydrogen peroxide and a weakly basic catalyst also in an organic solvent. Bending the plastic tube causes the inner tube to fracture, thus allowing the reactants to mix; and immediately, a bright light emission corresponding to the color of the fluorescence is observed.

The amount of visible light produced by a chemiluminescent reaction is best measured in terms of the light capacity, L_c, the time-integrated intensity in lumen-hours of light generated per liter of emitting solution.

$$L_c = C_M \times QY_{CL} \times P \times 4.07 \times 10^4$$

The light capacity is dependent on C_M, the molar concentration of the limiting reactant (the oxalic acid derivative), the chemiluminescent quantum yield, QY_{CL}, a photopic factor, P, which relates the sensitivity of the human eye to the spectral distribution of the emitted light and a constant to convert to the appropriate units. It has been estimated that one pound of a perfectly efficient chemiluminescent system could generate 173,000 lumen hours of light, equivalent to the output of a 40-watt incandescent bulb burning continuously for two weeks.[5] This potential will probably never be achieved in a practical system, but substantial progress has been made in the development of peroxyoxalate chemistry as an effective light source. The highest light capacity attained to date is an impressive 940 lumen-hours per liter. The Cyalume lightsticks typically generate from 25 (blue) to 500 (yellow) lumen-hours per liter of solution, the variation being primarily due to the differences in excitation efficiency and the photopic factors of the different color fluorescers used in each system.

The unique form and rugged nature of the chemical lightsticks has led to many applications which cannot be effectively served by electrically powered devices. For example, in areas where the possibility of explosion exists, chemical lights can be used safely since being a "cold" source of light no chance for ignition exists. Over the years an amazing variety of uses have developed. Examples of such diverse applications include emergency lights for power failures, portable lights for camping and back-packing, safety lights for jogging, lights for ship-board lines and underway replenishment operations, markers for life-vests and air-sea rescue operations, and lures for commercial fishing for swordfish and tuna. A developing market is the use as safety lights for children at halloween. Purely novelty uses have also been increasing in recent years.

A chemiluminescent system using water as a solvent would open up an entirely new area of applications which were not previously attainable with organic solvent-based chemistry. It can be envisioned that a chemiluminescent tablet might be developed which would produce light emission on contact with water. The tablet would contain only the active ingredients: the oxalic acid derivative, the fluorescer and a solid source of hydrogen peroxide such as sodium perborate.

The efficiency of such a solid-state composition can be defined in terms of "light density," the number of effective lumen-hours of light generated by a gram of the solid formulation. The light density, L_d, is determined by the factors in the following equation:

$$L_d = QY_{CL} \times P \times C \times E \times 4.04 \times 10^4/M$$

where QY_{CL} is the quantum yield of the chemiluminescent reaction, P is the photopic factor described above, C is concentration in weight percent of the oxalic acid derivative, M is the molecular weight of that material and E is an efficiency factor defining the proportion of useful light at some minimum brightness level as a fraction of the total light produced by the system. On the basis of previous research it should be possible to produce an aqueous chemiluminescent reaction with a QY_{CL} of 25 percent, a P value of 80 percent and an E of 70 percent. These values substituted into the above equation along with a value of 63 percent for C and a molecular weight of about 500 give a L_d of 6.9 lumen hours per gram of formulation. A comparison of the light density of this hypothetical tablet with a common LeClanche flashlight cell indicates the tablet would be more than 17 times more efficient on a light density basis. It would also be more than 173 times more efficient than the *Cyalume* green lightstick.

This hypothetical tablet would have the following advantages:

- High light density
- Rapid activation by water
- Long shelf-life when protected from humidity
- Low toxicity
- Absence of fire or explosion hazard
- Moderate cost.

For many of the applications water should be available from waste water or sea water as well as from taps or streams.

As mentioned above, most of the studies on the peroxyoxalate chemiluminescent reaction were carried out in organic solvents. A potential problem in an aqueous system is the competing hydrolysis reaction. Water, being a nucleophile, can attack the oxalic acid derivative in competition with hydrogen peroxide. An analysis of the relative reactivities of the hydroperoxide anion versus the hydroxide ion indicates that OOH should be more reactive by at least a factor of 10^4. This favorable reactivity is a result of the "alpha effect" common to nucleophiles with adjacent common heteroatoms such as hydrogen peroxide and hydrazine. The favorable reactivity ratio is fortunate since the hydrolysis product, oxalic acid, is known to be a strong quencher of the peroxyoxalate chemiluminescent reaction at concentrations as low as 10^{-4}M in organic solvents.

It was recognized early that considerable structural modification of the oxalic acid derivative and probably the fluorescer would be required for the optimum aqueous system. The oxalic ester SAPO was the initial compound to show any significant activity in water when formulated with a water soluble fluorescer, Rhodamine B.[6]

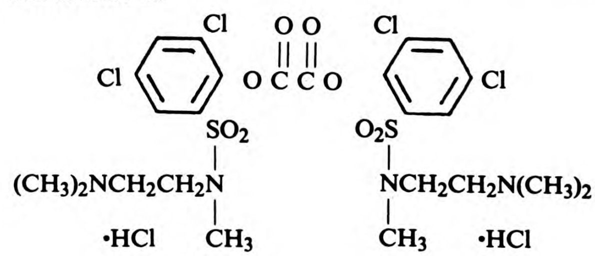

SAPO

This system on treatment with hydrogen peroxide in water gave a .004 percent quantum yield, a detectable level of emission which proved, in accordance with theory, that peroxyoxalate chemistry is feasible in aqueous media. However, the system was far from even approaching a practical light source. Some improvements were made by substituting a more efficient fluorescer, 8-hydroxy-1,3,6-pyrene trisulfonic acid, trisodium salt for the Rhodamine-B, bringing the quantum yield up to 0.008 percent.

It was evident at this stage of the research program that major changes in the structure of both fluorescer and oxalic acid derivative would be necessary to attain practical efficiencies in water. A synthetic program was undertaken to design and synthesize new structures for optimum efficiency in water.

Previous research had shown that certain oxalic sulfonamides gave significant reactivity in organic solvents.[7] While these amides would not be especially active in water, it was reasoned that more reactive sulfonamides might be of interest since the hydrolysis rate of these derivatives might be slower than the oxalic esters. The trifluoromethanesulfonyl (triflyl) group is known to be one of the strongest electron-attracting substituents,[8] so a series of water-insoluble triflyl oxamides (*3*) was prepared and found to be highly efficient in the non-aqueous reaction.[4] One member of this series was determined to be most efficient compound known with a chemiluminescent quantum yield of 34 percent in a phthalate solvent system. Table 1 summarizes the results on the trifylyoxamide series.

The data in Table 1 indicate that the triflyl group has a powerful activating effect on the oxamide. As indicated above, the unsymmetrical trichlorophenyl derivative was found to be the most efficient chemiluminescent compound known. The results from the two aliphatic oxamides, the 2-chloroethyl and the 2-methoxyethyl triflyloxamides, showed that the triflyl group was sufficently strong to give significant activity to compounds which would normally be virtually inactive. Based on these results, there was some encouragement that triflyloxamides could be prepared which would be soluble in water and hydrolytically stable while maintaining chemiluminescent activity.

A number of water-soluble triflyloxamides were prepared (compounds METQ, PETH and PETQ are examples) by treatment of the appropriate primary amine with triflic anhydride and oxalylation of the sulfonamide with oxalyl chloride in the presence of an acid acceptor.[9]

$$\mathrm{R\,CH_2CH_2\,\underset{T_f}{N}\,\overset{O}{\overset{\|}{C}}\,\overset{O}{\overset{\|}{C}}\,\underset{T_f}{N}\,CH_2CH_2\,R \cdot 2\,X^-}$$

$$\text{METQ: } \mathrm{R = \overset{CH_3}{\overset{|}{\underset{+}{N}}}(CH_2CH_2)_2O,\ X = OT_f}$$

PETQ: R = 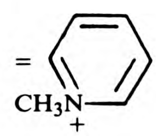 , X = OT_f

PETH: R = 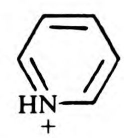 , X = Cl

These three oxamides gave significant quantum yields in the aqueous peroxyoxalate chemiluminescent reaction along with the water-soluble fluorescer rubrene sulfonate. Table 2 summarizes the results of these experiments. It was also found that addition of a nonionic surfactant gave a substantial increase in the efficiency of the chemiluminescent reaction.

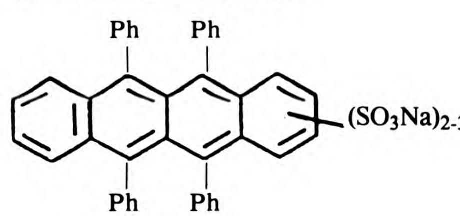

Rubrene Sulfonate

Table 1

Chemiluminescent Performance of N-Triflyloxamides[a]
$F_3CSO_2N(R(COCON(R)SO_2CF_3$ (*3*)

Compound	$QY^b_{CL} \times 100$	L^c_c
R = 4-Chlorophenyl	11.4	37.5
2,4-Dichlorophenyl	25.8	85.0
2,4,5-Trichlorophenyl	34.0	113.
2,4,6-Tricholorphenyl	12.5	41.1
4-Nitrophenyl	11.0	35.7
2-Methoxyethyl	2.85	9.2
2-Chloroethyl	3.68	12.2
2-Chloro-3-Pyridyl[d]	15.5	41.3

a. Chemiluminescent reactions contained .01M oxamide except where noted, 6.75×10^{-3}M 1-chloro-9,10-bis(phenylethynyl)anthracene, .375M hydrogen peroxide and 3×10^{-3}M sodium salicylate catalyst in a solvent mixture of 75 percent dibutyl phthalate, 20 percent dimethyl phthalate, 5 percent t-butanol.

b. Chemiluminescent quantum yield in einsteins per mole of oxamide.

c. Integrated visible light output in lumen-hours per liter.

d. Concentration of this oxamide was .008M.

The effect of the Deceresol NI surfactant, is illustrated in Figure 1 for the triflyl oxamide PETQ. It is evident that the surfactant increases both the efficiency and the lifetime, but no large differences in the rate of light decay were detected. A number of different classes of surfactant were evaluated in the aqueous chemiluminescent system. the nonionic polyoxyethylene types gave the best performance with the anionic sulfonates only slightly less effective. No improvement was found with cationic surfactants.

The mechanism by which the surfactant improves the efficiency of the chemiluminescent reaction is not known at present. However, one effect may involve protection of the fluorescer from photodegradation during the reaction. Rubrene, while known to be a highly efficient fluorescer in the non-aqueous reaction, is rapidly photoxidized at high concentration of hydrogen peroxide and oxalate ester. This limits the light capacity attainable from this fluorescer in organic solvents. It is known[10] that incorporation of a readily photoxidizable hydrocarbon into a micelle in water substantially retards the rate of photoxidation probably due to unfavorable kinetics of singlet oxygen migration and lifetime.

The structure of the fluorescer is vitally important in peroxyoxalate chemiluminescent chemistry. It appears to be even more critical in aqueous systems than in organic solvents. In high light capacity organic solvent-based systems derivatives of the 9,10-bis(phenylethynyl)-anthracene (BPEA) were the fluorescers of choice. A

Table 2

Aqueous Chemiluminescent Efficiency of Triflyl Oxamides[a]

Oxamide	Surfactant Conc.	$QY_{CL} \times 100$	L_c	T.75[b]
METQ	None	0.64	4.9	1.6
METQ	.001M	4.48	36.3	2.3
PETQ	None	1.45	11.6	6.0
PETQ	.001M	7.00	62.3	5.8
PETH	.001M	7.02	60.2	21.0

a. Chemiluminescent reactions contained 0.04M oxamide, the indicated concentration of the Deceresol NI nonionic surfactant .01M rubrene sulfonate and 1.75M hydrogen peroxide. See Table 1 for heading definitions.

b. Time required for 75 percent of the total light to be emitted.

Figure 1

Effect of surfactant on PETQ efficiency.

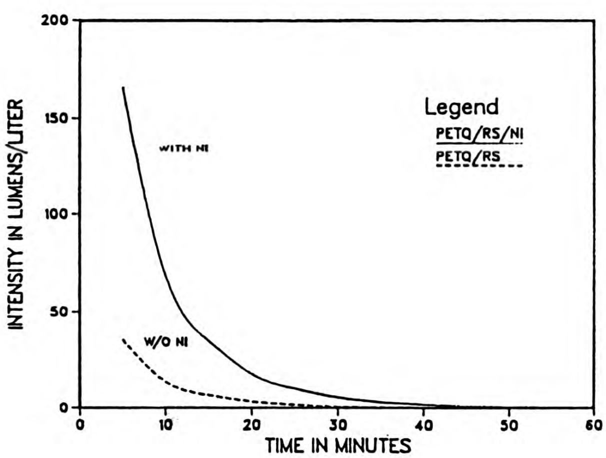

Table 3

Efficiency of Fluorescers in Water/Cyclohexane Emulsion[a,b]

Fluorescer	$QY_{CL} \times 100$	L_c	T.75
BPEA	0.12	1.1	11.5
1-Chloro-BPEA	0.12	1.3	8.0
2-Methyl-BPEA	0.45	4.9	10.8
2-Ethyl-BPEA	1.00	10.4	9.5
Bis-Octyl-BPEA	0.79	8.5	8.7
Rubrene	6.26	59.4	9.7
Tetrabromorubrene	6.74	46.7	9.3
Bis-Hexylrubrene	8.28	60.8	11.8
Bis-Dodecylrubrene	6.78	51.1	10.9

a. Reactions contained .003M of the BPEA derivatives, .01M of the rubrene derivatives, .04M METQ, 1.75M hydrogen peroxide and .001M Deceresol NI surfactant in a solvent mixture of 82 percent water and 18 percent cyclohexane by volume.

b. See Tables 1 and 2 for heading definitions.

number of water-soluble BPEA derivatives were prepared and as a group these compounds were much less effective than the rubrenes. Table 3 illustrates a comparison of these two classes in an aqueous emulsified solvent system with water-insoluble fluorescers.

The quantum efficiency attained by the reaction using bis-hexylrubrene in the solvent emulsified system is the most efficient aqueous chemiluminescent reaction yet reported. It is noteworthy that this fluorescer is *insoluble* in water whereas the oxamide is soluble in the aqueous phase. Hydrogen peroxide most probably reacts with the oxamide in the aqueous phase and the key intermediate thus formed migrates from the aqueous phase into the micelle containing the fluorescer. The exicted singlet state of the fluorescer is then generated within the micelle and emits in a typical fluorescence decay process. The slight differences between the efficiency of rubrene and the alkyl-substituted rubrenes is probably due to the poorer solubility of rubrene in cyclohexane.

The efficiency of the aqueous systems described here falls substantially short of the target quantum yield of 25 percent in water. However, there is no question that practical aqueous chemiluminescent systems based on peroxyoxalate chemistry are possible. Even though the horizon is visible, considerable research and development effort will be required to achieve this goal.

References

1. Rauhut, M. M. Kirk-Othmer, *Encyclopedia of Chemical Technology,* 3rd. Edition, *5,* pp. 437-438.

2. Schuster, G. B., and K. A. Horn in "Chemical and Biological Generation of Excited States," Editors W. Adam and G. Cilento, Academic Press, New York, 1982 pp. 229-247.

3. Chandross, E. A., *Tetrahedron Letters* (1963) p. 761.

Rauhut, M. M. *Accounts of Chemical Research,* 2 (1969) p. 80.

4. Tseng, S. S., A. G. Mohan, L. G. Haines, L. S. Vizcarra and M. M. Rauhut, *Journal of Organic Chemistry,* 44 (1979) p. 4113.

5. Rauhut, M. M., "Chemiluminescence and Bioluminescence," Editors M. J. Cormier, D. M. Hercules and J. Lee, Plenum Press, New York (1973) pp. 451-460.

6. Mohan, A. G., R. Dulina and A. A. Doering, "Investigation of Water-Soluble Chemiluminescent Materials," Final Report to the National Aeronautics and Space Administration, Contract NSA 5-22303 (1976).

7. Maulding, D. R., R. A. Clarke, B. G. Roberts and M. M. Rauhut, *Journal of Organic Chemistry, 33* (1968) p. 250.

8. Hendrickson, J. B., D. B. Sternbach and K. W. Blair, *Accounts of Chemical Research,* 10 (1977) p. 306.

9. Mohan, A. G., *et al.,* Final Report to the Office of Naval Research, Contract N00014-77-C-0634 (1982).

10. Turro, N. J., M. Gratzel and A. M. Braun, *Angewandte Chemie International Edition in English,* 19 (1980) p. 675.

Acknowledgements

The authors would like to express their appreciation to their coworkers in the Chemical Research Division of the American Cyanamid Company. The generous support and encouragement of the Office of Naval Research, in particular Dr. George Neece and Dr. Rudy Marcus is gratefully acknowledged.

Authors

Dr. Arthur G. Mohan has been involved in chemiluminescence research under a number of ONR contracts as a project leader and principal investigator while at American Cyanamid. He currently is Adjunct Professor of Chemistry at Seton Hall University. Most recently Dr. Mohan has authored a chapter in *Chemiluminescence and Bioluminescence Today* to be published by M. Dekker in the fall of 1984.

Dr. Michael M. Rauhut has been one of the "leading lights" of chemiluminescence since the early days of basic research under Navy sponsorship in the mid-sixties. He has published extensively in the field and is one of the discoverers of the peroxyoxalate system. Dr. Rauhut holds over 30 patents in the field of chemiluminescence and currently is a research manager in American Cyanamid's Chemical Research Division in the Stamford, Connecticut laboratories.

ARCTIC

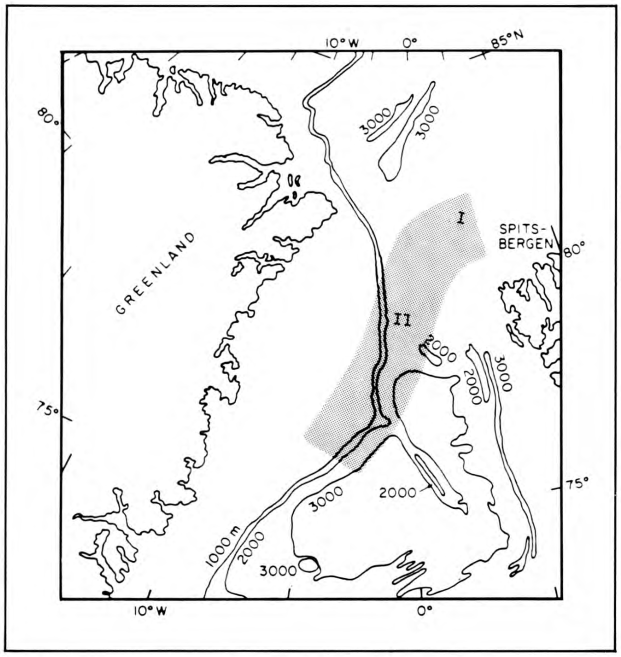

Marginal Ice Zone Experiment

Scientists from ten nations, including the United States, conducted the most extensive environmental field study every undertaken of the Arctic region this past summer.

Spending six weeks in the northermost Greenland Sea, scientists from West Germany, France, Denmark, Finland, Norway, Switzerland, Ireland, Canada, England and the U.S. studied how ice, water and atmosphere interact at the edge of ice.

Each season the edge or open boundaries of the polar icefield migrates as much as 375 miles in a north-south direction. This change affects the weather patterns of the entire northern hemisphere and has a significant effect on naval operations and commercial fisheries.

Primarily funded by the Office of Naval Research (ONR), the study, known as the Marginal Ice Zone Experiment (MIZEX), was designed as a drifting experiment, covering approximately 125 square miles of the East Greenland Sea.

The overall program is built around a series of major observational field studies or MIZEX's, the one for the summer of 1984 is described in this paper. A pilot program was held in 1983 (MIZEX 1983). Both MIZEX's were conducted in the summer months whereas the follow-on experiments in 1986-1987 will be in the winter.

For conceptual and organizational clarity, the MIZEX effort can be broken into seven subgroups: remote sensing, meteorology, ice, oceanography, biology, modeling, and acoustics. Some of the major problems and proposed work in each discipline are described below; more complete descriptions may be found in Wadhams[1] and Johannessen.[2]

Remote Sensing

Given the extent and inaccessibility of areas affected by the MIX, remote sensing is the only practical way of applying increased understanding from experiments like MIZEX to long-term monitoring and routine prediction of ice-edge characteristics. Eddy-like structure along the ice edge in the Greenland Sea has been shown by LANDSAT images. Similar images have been attained with microwave sensors demonstrating the feasibility of all-weather all-season remote observation.[3] If MIZEX succeeds, for example, in providing reasonable estimates of cross-edge heat and mass exchange in eddy or banding processes, then routine surveillance of such features will provide much improved estimates of large scale heat and mass budgets.

From an experimental standpoint, remote sensing provides the overall view necessary to identify special features for intensive study. Because persistent cloudiness is anticipated, microwave sensors (SAR, SLAR, and passive microwave) will be used extensively. Studies of ice deformation obtained by tracking identifiable natural and artificial targets will complement buoy and transponder measurements.

Meteorology

The lower boundary of the atmosphere across the MIZ changes from a maritime regime, with low albedo and moderate temperature, to a highly reflective and, during much of the year, very cold regime. These changes, combined with dramatic variation in surface roughness, can impose large gradients in radiative fluxes, in surface stress, and in turbulent moisture and heat fluxes. Over pack ice, the boundary layer is usually stabbly stratified, with low, strong inversions. If this cold air is advected over open water with a strong temperature contrast, turbulence is intensified. By the same token, warm air advected over the cold surface is stabilized, with decreasing turbulence levels. Ice is generally thought to be rougher than the ocean surface, so that for the same surface wind and stability, turbulent drag over pack ice is greater than over the open sea; furthermore, roughness of the ice itself is often increased within the MIZ by rafting and pulverization. Sorting out these various effects presents a considerable challenge but is important for understanding how the ice and underlying water respond to the wind.

The MIZEX experiments employed a variety of meteorological instruments for surface layer studies, deployed from ships and ice floes, along with aircraft boundary-layer measurements, radiosonde launchings, acoustic sounders, closely spaced surface pressure arrays, and buoy-mounted weather stations. An active atmospheric modeling component complemented the field measurements.

Ice

Sea-ice studies in the MIZ divide roughly into two classes: one concerned primarily with the thermodynamic growth, decay, and internal structure of ice; the other concerned with the mechanical properties of sea ice as a material affected by dynamical forces, mainly wind and current.

Ice in the MIZ is broken into much finer individual floes and pieces than are found in the interior pack. Attenuation of surface wave energy by the pack ice is certainly a major factor in this break-up; gradients in other forces, such as horizontal current shear, may also contribute. These interstitial areas of open water not only change the mechanical properties of the ice, but also modify the radiation balance and the mean surface temperature sensed by the atmosphere. In summer, melt rates may be enhanced by increased insulation between floes; in winter, ice production is increased by continual opening and closing.

Water near the margin may contain more sensible heat than is usually found in the Arctic mixed layer, giving oceanic heat flux a greater role in the thermodynamic energy balance that controls ice thickness. The mass balance of ice regulates buoyancy flux into the oceanic boundary layer; thus, if oceanic sensible heat is available, the growth rate can serve as an important feedback parameter.

Kinematics of ice motion in the MIZ are also of much interest. Buoy and satellite imagery studies indicate comparatively large shear normal to the ice edge and divergence along the East Greenland Drift Current. MIZEX will also study attenuation of inertial and tidal oscillatory motion.

Measurements completed included detailed studies of changes in mass, concentration, and floe size distribution, along with energy budget observations and properties of ice measured both in situ and cored for more extensive laboratory analysis. Radar positioning techniques and satellite navigation were used to study kinematics of the ice drift field with an array of drifting buoys. In addition, mean motion, wave and collision accelerations, ablation, and other properties were studied at the extreme ice edge, including eddies and bands.

Oceanography

Modification of the upper ocean across the ice edge is often extreme, with large changes in temperature and salinity, large horizontal gradients in vertical density structure (with corresponding geostrophic shear), and rapid variation in surface momentum and buoyancy flux. At times, the MIZ coincides with the surface manifestation of a permanent, oceanic front (e.g., the East Greenland Polar Front), which may in turn be tied to a topographic feature (the shelf break); but as is the case in many marginal seas and in most of the Southern Oean, the ice edge itself often forms a rapidly migrating, oceanic frontal zone. These fronts exhibit a variety of interesting features: eddies,[3] fine structure,[4] jets, and meanders. A summertime Soviet project at the Chukchi Sea MIZ noted a jet, directed along the ice edge so that open water was on the right, that persisted for the duration of the experiment regardless of wind direction.[5] The jet, which meandered on scales of about 90 km, probably resulted from geostrophic adjustment between relatively warm and saline water from the south and a lens of water freshened by ice melt.

Ice-edge upwelling and other mesoscale circulations appear in the MIZ; they are thought to be driven by surface gradients in stress or buoyancy flux. The Chukchi ice-edge jet mentioned above seems to fall in the latter class, since it was apparently independent of local wind. On the other hand, Buckley[6] observed a large upwelling event north of Svalbard in early winter which they attributed to a surface stress gradient much like coastal upwelling. In this case it is hypothesized that sea ice, because of its greater upper surface roughness, imparts more momentum to its underlying boundary layer, causing Ekman divergence at the ice edge.

Boundary layer and surface layer processes are also an active area of research. Rapid melting at the ice margin can yield in the upper ocean an input of fresh water at a rate comparable to that of a torrential rainfall, creating a stable boundary layer analogous to the nocturnal boundary layer of the atmosphere. McPhee[7] suggests the resulting reduction in drag on the ice underside as an explanation for divergence of bands of sea ice away from the main pack under off-ice winds. Absorption and reflection of surface gravity wave energy is also a significant factor in the MIZ, invoked to account for the relatively sharp ice edge often observed. Wave radiation stress has also been suggested as a primary factor in the formation of ice-edge bands.[8]

Figure 1

MIZEX 84 program overview.

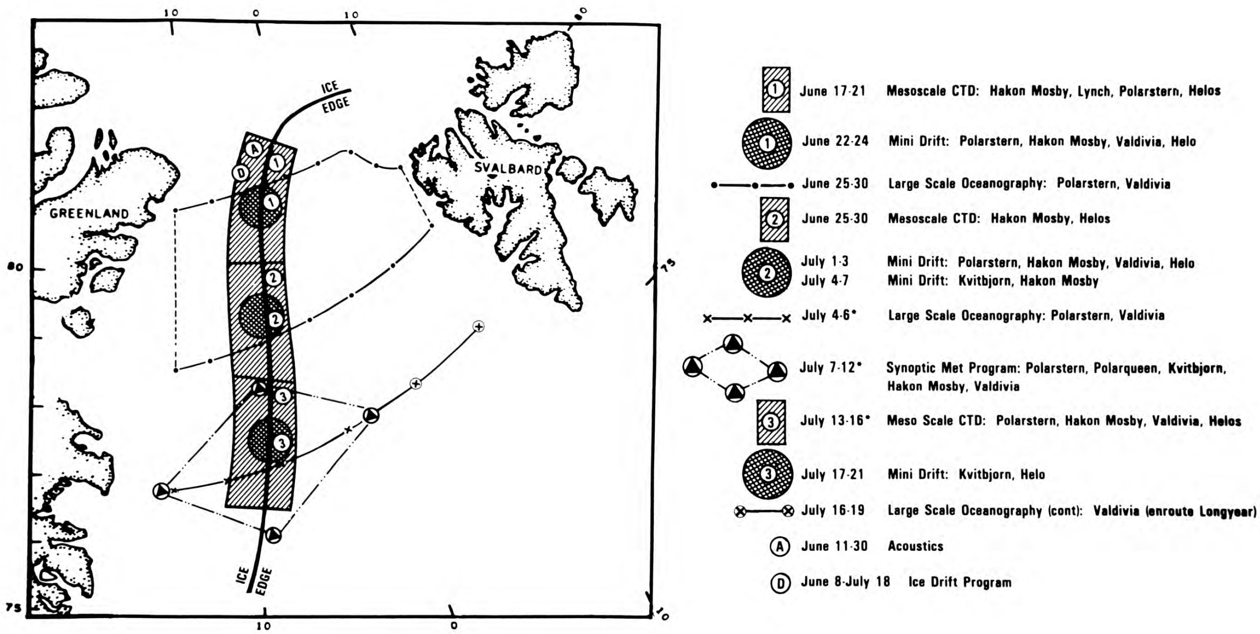

An ambitious oceanographic measurement program was conducted during the MIZEX experiments, including current meter moorings, both bottom anchored and suspended from the surface; extensive hydrography from ship and helicopter; profiling current meter systems; boundary layer turbulence measurements; expendable temperature and velocity probes; high frequency acoustic sounding; and Doppler acoustic current meter mapping. In addition, surface and perhaps subsurface drifters were deployed with CODAR measurements of surface velocity on each side of the ice margin. Tracer studies, which have recently been used to identify residence times of sub-surface water north of Fram Strait[9] were extended to the MIZ.

Biology

In high latitude biological systems, the ice edge region has higher levels of primary productivity than surrounding waters. Alexander[10] shows that over a third of the total primary productivity in the southeast Bering sea comes in the single month of May, coinciding with the ice edge bloom. Associated with the bloom is a concentration of marine mammals and birds at the ice edge, with some species adapted specifically to the ice-edge habitat. There are several competing hypotheses for the presence of the bloom, among them: a) a benevolent environment furnished by a shallow, high-nutrient, mixed layer stabilized by melt water; and b), increased nutrient levels associated with ice-edge upwelling. Recent work describing the halocline of the Arctic Ocean has emphasized the role of the broad Arctic shelves in maintaining the cold, saline layer of water that separates the relatively fresh Arctic mixed layer from underlying Atlantic water.[11] Presumably, modified shelf water upwelled by processes at the ice edge could supply the needed elevated nutrient levels. If such upwelling is intermittent, the biological signal from each even may provide a 'memory' that is lacking in measurements of the physical properties alone.

Biological measurements in MIZEX included phytoplankton biomass, phytoplankton species, nutrients, zooplankton biomass and diversity, and a variety of chemical components.[12]

Modeling

Credible models of MIZ processes across the whole range of disciplines is a major goal in the MIZEX effort. A partial list includes: sea-ice radiation, thermodynamics, ridging, breaking, and rheology; atmospheric

Figure 2

MIZEX 1984 acoustics experimental plan.

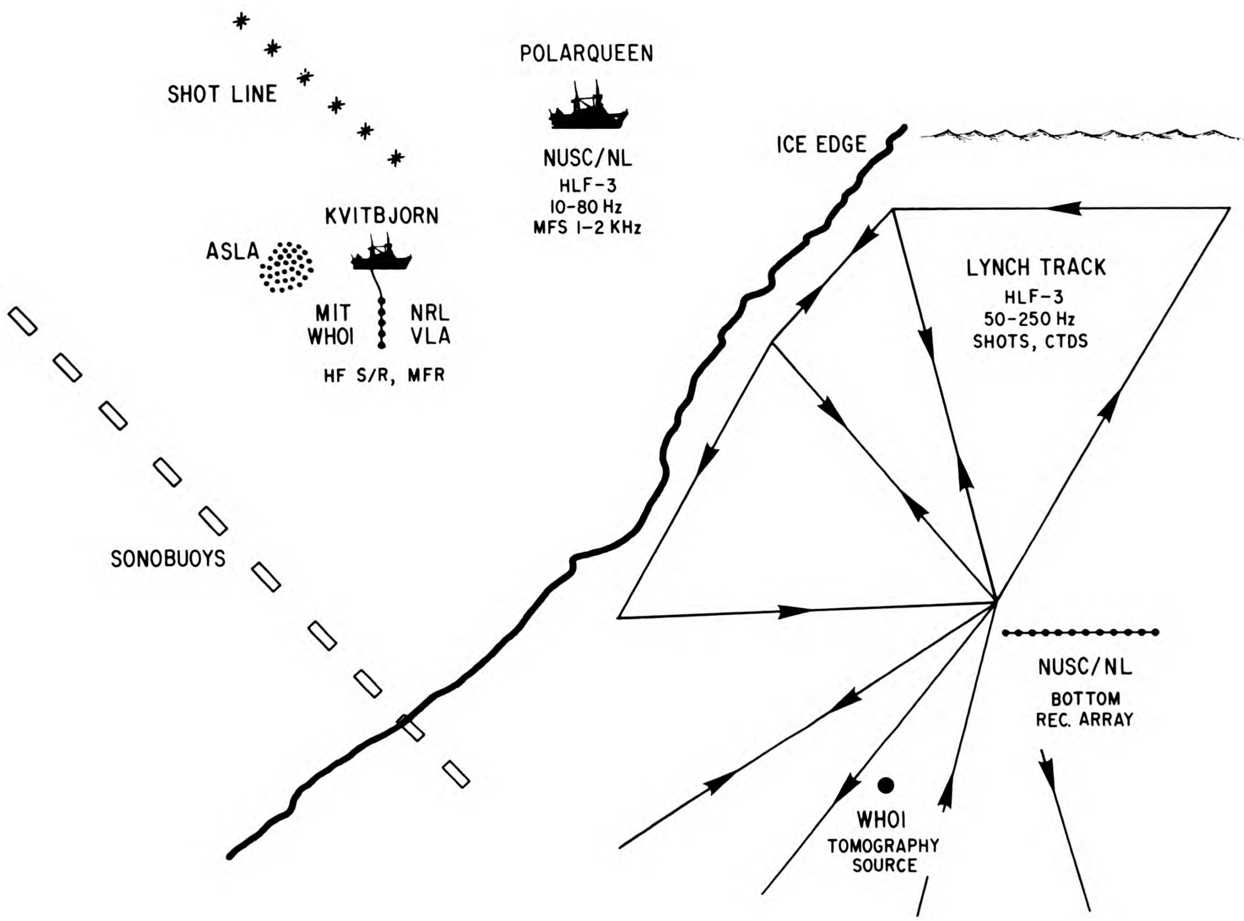

and oceanic boundary layers; eddy generation; frontogenesis and maintenance of fronts; quasisteady, mesoscale circulations in atmosphere and ocean; fine structure and cross-frontal mixing; biological processes; internal waves; sound path and acoustic tomography; and many others. In addition to their role as end products, models were used prior to the experiment and in the field to optimize sampling strategies.

Acoustics Program

The MIZEX 84 acoustics plan is of particular interest as some elements of the program address issues relevant to Arctic ASW. The general geographical location of the MIZEX 84 acoustics experiment is shown as (A) in Figure 1. The experiment began in June, 1984, and lasted approximately two months. A detailed plan of the experiment is illustrated in Figure 2. The principal ship for the acoustic program was the MV KVITBJORN. It served as a drift ship positioning itself at a distance of at least 30 km in from the edge of the ice and at least 30 km laterally away from the MV POLARQUEEN. One helicopter and a crew of one pilot and one pilot/mechanic were stationed with the KVITBJORN continuously during this phase both in support of the activities local to the KVITBJORN and to operate acoustic stations away from the KVITBJORN.

The basic MIZEX 84 acoustic objectives involved work in essentially seven areas: 1) ambient noise; 2) propagation studies; 3) high frequency (30 to 60 kHz) forward- and backscattering measurements from the under ice surface; 4) basin and ice reverberation; 5) seismic reflection profiles; 6) seismic refraction profiles; and 7) a tomography demonstration test.

In addition to this rather complete suite of acoustical measurements, a key element of the MIZEX 84 effort was a tomographic feasibility test. This was performed by WHOI (Woods Hole Oceanographic Institution) and involved transmitting 224 Hz pulsed pseudorandom sequences from a moored source to the NRL vertical array at a range of some 130 to 150 km. The purpose of this test was to demonstrate the crucial acoustic elements for the application of acoustic tomography: that the multipath arrivals which have experienced numerous bounces off the ice/water surface are resolvable, stable, and identifiable. To date, tomography has been demonstrated only for deep ocean propagation where the eigenrays connecting the source and receiver have not interacted with the ocean boundaries. If succesful, the test will have far reaching implications not only for conducting tomographic experiments in the Arctic, but for other regions as well.

The MIZ is a significant region in two senses, firstly as a location for man's activities and secondly as an important geophysical boundary zone involving energy exchanges which require parameterization in large-scale ocean-atmosphere models. This area is subject to fluctuations due to short-term forcing such as cyclone passages and eddy generation and to longer-term factors (seasonal and interannual). Successful modeling and prediction of variations in ice edge position and ice concentration will be of great value in furthering man's activities in the region.

For more information about MIZEX, contact Dr. G. Leonard Johnson, Code 425 AR, Office of Naval Research, Arlington, Virginia, 22217; or telephone (202) 696-4118.

References

1. Wadhams, P. S., S. Martin, O. M. Johannessen, W. D. Hibler, III, and W. J. Campbell (Editors), "MIZEX, A Program for Mesoscale Air-Ice-Ocean Experiments in Arctic Marginal Ice Zones I, Research Strategy," U.S. Army Cold Regions Research and Engineering Laboratory, Special Report 81-19 (1981).

2. Johannessen, O. M., W. D. Hibler, III, P. Wadhams, W. J. Campbell, K. Hasselman, and I. Dyer (Editors), "MIZEX, a Program for Mesoscale Air-Ice-Ocean Interaction Experiments in the Arctic Marginal Ice Zone. II. A Plan for a Summer Marginal Ice Zone Experiment in the Fram Strait/Greenland Sea: 1984," U.S. Army Cold Regions Research and Engineering Laboratory, Hanover, N.H., (1983).

3. Johannessen, O. M., J. A. Johannessen, J. Morison, B. Farrelly, and E. Svendsen, "Oceanographic Conditions in the Ice Edge Region North of Svalbard in Early Fall 1979 With an Emphasis on Mesoscale Processes," *Journal of Geophysics Research 88* (1983) p. 2755.

4. Paquette, R. G. and R. H. Bourke, "Ocean Circulation and Fronts as Related to Ice Melt-back in the Chukchi Sea," *Journal of Geophysics Research, 86,* (1981) p. 4215.

5. Nikolaev, S. G., "Experiment in Organizing Oceanographic Investigations of the Ice Edge Zone of the Chukchi Sea," *Problemy Arktikii Antarktiki, 42,* (English Translation) (1973) p. 31.

6. Buckley, J. R., T. Gammelsrod, A. Johannessen, O. M. Johannessen and L. P. Roed, "Upwelling: Oceanic Structure at the Edge of the Arctic Ice Pack in Winter," *Science 203* (1979) p. 165.

7. McPhee, M. G., "Greenland Sea Ice/Ocean Margin," EOS, *Transactions of American Geophysical Union) 64* (1983) p. 82.

8. Wadhams, P. A., "A Mechanism for the Formation of Ice Edge Bands, *Journal of Geophysics Research 88* (1983) p. 2813.

9. Ostlund, H. G., Z. Top and V. E. Lee, "Isotope Dating of Waters at Fram III," *Geophysics Research Letters 9* (1982) p. 1117.

10. Alexander, V., "Interrelationships Between the Seasonal Sea Ice and Biological Regimes," *Cold Regions Science and Technology, 2,* Edited by B. Andersen, W. F. Weeks and J. J. Newton (1981).

11. Aagaard, K., L. K. Coachman and E. Carmack, "On the Halocline of the Arctic Ocean," *Deep Sea Research 28A* (1981) p. 529.

12. McPhee, M. G., "Turbulent Heat and Momentum Transfer in the Oceanic Boundary Layer Under Melting Pack Ice," *Journal of Geophysics Research 88* (1983) p. 2827.

Research Notes

New Missile Dome Materials

High speed tactical missiles employing infrared or multimode guidance for the 1990 time frame will be feasible only if the following materials problems can be solved: a) rain erosion/thermal shock resistance, b) reduced thermal emission, c) multimode operation. Recently ONR sponsored work at General Telephone and Electronics (GTE) has produced a new missile dome material that should have substantial impact on these problems.

The program at GTE has discovered a unique method to prepare optically transparent missile dome materials. The method is unique in the sense that the material system (La_2O_3-Y_2O_3) is sintered to theoretical density in a two phase field and then annealed back to a partially single phase material to optimize the infrared transmission and mechanical properties. Powders of La_2O_3 and Y_2O_3 were prepared from chemical preparation methods. Jet milling was used to reduce agglomeration. The powders were then isostatically pressed and sintered to near theoretical density. The resulting materials had near theoretical transmittance in the 3-5 micrometer band and had nearly twice the fracture toughness of existing materials. Such an increase in fracture toughness should result in substantial erosion resistance. The material also had an order of magnitude less thermal emission than existing materials.

This newly developed missile dome material could permit the development of missiles with multimode guidance (radar and IR 3-5 micrometer). Further, the thermal emission of this material is one of the lowest for 3-5 micrometer IR materials. Thus, focal plane array technology for the detector which requires such a property may be possible. Finally, the improved mechanical properties should permit increased missile performance and all weather capability.

In summary, a unique material process was discovered that produced a potentially superior missile dome material with respect to rain erosion resistance and thermal emission. Further, the material has the potential to permit multimode operation and should significantly advance future high speed tactical missile capability.

(Robert C. Pohanka, ONR)

Significant Advance in Welding Fluxes for Titanium

The Office of Naval Research (ONR) has been pursuing new formulations of weld fluxes that permit high-deposition electroslag and submerged-arc welding of titanium alloys. *At the present time no flux is available in the United States that can produce acceptable low oxygen defect-free welds in titanium.* ONR research at the Massachusetts Institute of Technology (MIT), however, has established some of the basic thermodynamic criteria associated with titanium electroslag welding and provided the scientific basis for a program at the Oregon Graduate Center. The research at MIT on gas-metal-slag equilibria has shown that CaF_2 is required as the base flux composition for electroslag welding of titanium. This gives the appropriate melting point and prevents oxygen and nitrogen contamination of the weld metal. However, the MIT reserach also indicates that the CaF_2 flux can have problems: it can give welding arc instabilities requiring that the process be monitored continuously; it can produce a rough weld bead surface and an undesirable high weld bead contact angle with the base plate, and, because of the high conductivity of the CaF_2 flux, high weld currents (1000-1200 amperes) are required to melt the titanium, putting severe requirements on the available welding power supplies. Based on this past MIT experience, Dr. J. Devletian (Oregon Graduate Center, Beaverton, Oregon) under Naval Sea Systems Command funding set out to examine the effects of additives to the CaF_2 flux with the objective of increasing electrical resistivity for more effective heating. Recently, Dr. Devletian made a significant breakthrough by formulating a new flux composition that appears to solve many of the previous problems encountered. This new flux brings immediate order to the welding process, ending arc instabilities. Furthermore, the decreased electrical conductivity of the flux permits lower welding currents. This opens up for the first time the distinct possibility of electroslag and submerged arc welding of titanium alloys.

(Bruce A. MacDonald, ONR)

Sea Marc II

Sea MARC II is a long-range, side-scan sonar system, developed with funding from the Office of Naval Research, which produces an acoustic image of the seafloor. In addition, the system has the unique capacity of being able to measure the direction of the seafloor reflection. When the range along with this direction are accurately determined, these data can be calculated for the ensonified swath of seafloor. Thus, the Sea MARC II system provides the equivalent of an aerial photograph of the seafloor accompanied by a high resolution bathymetric map, for naval applications such as obstacle avoidance.

Sea Marc II employs a transducer array that is towed at a shallow depth, typically 100 meters below the sea surface. The system operates at 12 kHz on the starboard side and 11 kHz on the port side. Towing the array is desirable because it permits operation of the system from a relatively small and inexpensive vessel and because it provides greater stability than can be obtained when the array is attached to the hull of a surface vessel. The width of the swath of seafloor ensonified is proportional to the water depth, and presently is 3.4 times the depth. In 4500 meters of water this allows swath coverage of 15 km. While the array has been tested at speeds of up to 18.5 km/hr (10 knots) more typical tow speeds are 15 km/hr (8 knots). At these speeds and allowing for swath overlap, over 3000 sq km of seafloor can be surveyed on a daily basis.

With the first scientific cruises of high resolution bathymetric devices such as Sea MARC II, important break-throughs in the understanding of earth crust dynamics were made. An example is the concept of overlapping spreading centers, which simply stated, is a case of the earth's crust moving at different speeds in a localized area.

(Gerald B. Morris, ONR)

Fiber Optic Pulse Compression

Under an Office of Naval Research (ONR) contract, Dr. Dan Grischkowsky of IBM Research Laboratories in Yorktown Heights, New York, has developed a generalized technique for compressing the pulses from a pulsed laser to produce shorter duration optical pulses. This new technique is simple, can be used over a continuous range of wavelengths extending from the visible through the near infrared spectrum, and does not require high optical powers. Very recently, this technique has been used to produce the shortest duration optical pulses ever measured.

Very short optical pulses from a pulsed laser can be further shortened by passing these pulses through an optical pulse compressor. The optical pulse compressor consists of an optical fiber which is about 30 meters in length and has a diameter of 4 microns. (The length of fiber used depends on the pulse duration from the laser.) The optical output from this fiber is a pulse whose frequency is continuously changing in a very controlled way from the beginning to the end of the pulse. At the point at which this pulse exits the fiber, the pulse is somewhat longer than the original starting pulse. However, because of the controlled manner in which the pulse has been lengthened and its frequencies changed, it can now be significantly compressed by passing it through a dispersive delay line. A dispersive delay line is a "device" which introduces a delay in the output pulse which depends on the instantaneous frequency of the input pulse at any instance of time. In this case, the dispersive delay line consists of two optical gratings which are aligned such that the frequencies of the first part of the pulse require that portion of the pulse to travel a greater distance than subsequent parts of the pulse. The result is that the pulse becomes compressed. This technique was developed at IBM under an ONR contract and used to compress an 8 picosecond pulse to 120 femtoseconds using two stages of pulse compression. That is, the first stage compressed the 8 picosecond pulse to 240 femtoseconds and the second stage provided an additional compression factor of 2 to give a 120 femtosecond pulse. It has been subsequently used at Bell Laboratories where extremely short pulse lasers are available and produced 60 femtosecond pulses. These short optical pulses are less than .02 millimeters in length. The same technique was used very recently by researchers at the Massachusetts Institute of Technology to produce pulses of 16 femtoseconds duration, the shortest on record.

This work is important to the Navy because it will significantly impact the study of ultrafast relaxation processes. The details of ultrafast electron-dynamics in solids and on surfaces are essential to a more complete understanding of the basic processes occurring in these systems and ultimately to the development of new materials for improved electronic and electrooptic devices. In addition, it has recently been shown that optical pulses can be converted with good efficiency to X-rays and it now becomes possible to think seriously about using ultrashort duration X-ray pulses for a wide range of applications.

Because this technique is simple, it can be used over a wide range of wavelengths, does not require high optical powers, and it will become the standard technique for producing ultrashort optical pulses in laboratories throughout the world!.

(Herschel S. Pilloff)

Corrections Noted

Corrections for Naval Research Reviews, Three/1983, Vol. XXXV, (special issue on the Naval Weapons Center) are noted below:

Page 7, right column beginning on line 16: "One hypothesis to explain the uplift and geodetic deformation *along the track* is . . ." should read "One hypothesis to explain the uplift and geodetic deformation *in the Coso Range* is . . ."

Page 19, below photo: *G. E. McManis* of NWC should have been listed as third author of "New Concepts in Thermal Batteries."

Page 31, third line from bottom: "*trans*-1,3,5,7- . . ." should read "*cis*-1,3,5,7- . . ."

Page 31, second line from bottom: "prepared from 1,2,3,4- . . ." should read "prepared from *meso*-1,2,3,4- . . ."

Page 33, left column, first line: "The isomeric *cis*-1,3,5,7- . . ." should read "the isomeric *trans*-1,3,5,7- . . ."

Page 37, second column, line 31: "However, in SEXAFS techniques surface sensitivity is provided by detecting the photoelectron yield (PEY), *instead of the transmitted x-rays resulting from soft x-rays excitation.*" should read "However, in SEXAFS techniques surface sensitivity is provided by detecting the photoelectron yield (PEY) *resulting from soft x-ray excitation, instead of the transmitted x-rays.*"

Page 38, line 24: "$Z < 10$eV)" should read "($E < 10$eV)"

Page 40, Figure 3: The figure shows that the line marked with circles is CLEAVE NO. 1 and the one marked with squares is H_2O -DOPED. That should be reversed; the line marked with circles is actually H_2O - DOPED and the one marked with squares is CLEAVE NO. 1. In the caption accompanying that figure, the H* occurring in the first and sixth line should be H^+.

DEPARTMENT OF THE NAVY
OFFICE OF NAVAL RESEARCH
ARLINGTON, VA. 22217

OFFICIAL BUSINESS
PENALTY FOR PRIVATE USE, $300

THIRD-CLASS MAIL
POSTAGE & FEES PAID
USN
PERMIT No. GS-9

Marginal Ice Zone Experiment